Differential endocytosis and signaling dynamics of insulin receptor variants IR-A and IR-B

Jimena Giudice[1,2], Federico Coluccio Leskow[2], Donna J. Arndt-Jovin[3], Thomas M. Jovin[3,4] and Elizabeth A. Jares-Erijman[1,*]

[1]Departamento de Química Orgánica, Facultad de Ciencias Exactas y Naturales (FCEN), Universidad de Buenos Aires (UBA), CIHIDECAR, CONICET, Intendente Güiraldes 2160, Ciudad Universitaria, C1428EGA, Buenos Aires, Argentina
[2]Departamento de Química Biológica, FCEN, Universidad de Buenos Aires (UBA), Intendente Güiraldes 2160, Ciudad Universitaria, C1428EGA, Buenos Aires, Argentina
[3]Laboratory of Cellular Dynamics, Max-Planck Institute for Biophysical Chemistry (MPIbpc), D-37077 Göttingen, Germany
[4]Laboratorio de Dinámica Celular, Facultad de Ciencias Exactas y Naturales (FCEN), Universidad de Buenos Aires (UBA), Intendente Güiraldes 2160, Ciudad Universitaria, C1428EGA, Buenos Aires, Argentina
*Author for correspondence (eli@qo.fcen.uba.ar)

Accepted 26 October 2010
Journal of Cell Science 124, 801-811

doi:10.1242/jcs.076869

Summary

Insulin signaling comprises a complex cascade of events, playing a key role in the regulation of glucose metabolism and cellular growth. Impaired response to insulin is the hallmark of diabetes, whereas upregulated insulin activity occurs in many cancers. Two splice variants of the insulin receptor (IR) exist in mammals: IR-A, lacking exon 11, and full-length IR-B. Although considerable biochemical data exist on insulin binding and downstream signaling, little is known about the dynamics of the IR itself. We created functional IR transgenes fused with visible fluorescent proteins for use in combination with biotinamido-caproyl insulin and streptavidin quantum dots. Using confocal and structured illumination microscopy, we visualized the endocytosis of both isoforms in living and fixed cells and demonstrated a higher rate of endocytosis of IR-A than IR-B. These differences correlated with higher and sustained activation of IR-A in response to insulin and with distinctive ERK1/2 activation profiles and gene transcription regulation. In addition, cells expressing IR-B showed higher AKT phosphorylation after insulin stimulation than cells expressing IR-A. Taken together, these results suggest that IR signaling is dependent on localization; internalized IRs regulate mitogenic activity, whereas metabolic balance signaling occurs at the cell membrane.

Key words: Insulin, Insulin receptor isoforms, Programmable array microscope, Quantum dots

Introduction

Insulin signaling comprises a complex cascade of events, playing a key role in the regulation of glucose metabolism and in cellular growth. Impaired response to insulin is the hallmark of diabetes, whereas upregulated insulin activity occurs in many cancers (Papa et al., 1990; Baillies et al., 1997; Pandini et al., 1999; Saltiel and Kahn, 2001; Pandini et al., 2002). Insulin binds to specific receptors at the cell surface, triggering their phosphorylation and thereby activating downstream signaling pathways with concomitant receptor internalization and recycling. The long-term consequences of insulin binding result in increased cell growth and gene expression. However, how receptor dynamics and redistribution regulate the transport and metabolism of glucose, lipids and proteins is not understood in detail.

The insulin receptor (IR) belongs to a subfamily of receptor tyrosine kinases (RTK) that includes the insulin-like growth factor (IGF) I receptor (IGF-1R) and the insulin-receptor-related receptor (Ebina et al., 1985; Seino and Bell, 1989; Patti and Kahn, 1998). The receptors are tetrameric proteins consisting of two extracellular α-subunits and two transmembrane β-subunits linked by disulfide bonds.

The human IR is encoded by a single *INSR* gene comprising 22 exons. Alternative splicing of exon 11 (Seino and Bell, 1989) gives rise to two protein isoforms differing by a 12-amino-acid insert in the hormone binding domain at the C-terminus of the α-subunit: IR-A (lacking exon 11) and IR-B (with exon 11) (Ullrich et al., 1985; Ebina et al., 1985). The relative abundance of the two transcripts is regulated in a highly tissue-specific manner conserved among mammals (Goldstein and Dudley, 1990), suggesting that functional differences between the two isoforms might underlie the tissue-specific insulin action in vivo.

Although all cell types express both IR isoforms to various degrees, IR-A predominates in fetal tissues and cancer cells, and IR-B in adult differentiated cells. In embryos, IR-A promotes growth owing to its ability to bind insulin and IGF-II; in adults, IR-B is expressed predominantly in insulin-sensitive tissues regulating glucose homeostasis. Misregulation of IR alternative splicing is involved in some diseases and has important consequences for insulin and IGF-II sensitivity and responsiveness (Mosthaf et al., 1990; Mosthaf et al., 1991; Kellerer et al., 1993; Savkur et al., 2001; Sen et al., 2009).

IR-A has a higher affinity for insulin than IR-B. Furthermore, IGF-II binds to IR-A but not to IR-B, with an affinity close to that of insulin, whereas the affinity for IGF-I for both receptors is similar (Mosthaf et al., 1991; Yamaguchi et al., 1991; Yamaguchi et al., 1993; Frasca et al., 1999; Pandini et al., 2002; Benyoucef et al., 2007). Contradictory results were reported in mouse 3T3 cells using a targeted ablation of the *IGF-1R* gene (Denley et al., 2004). The fact that these studies were performed in different cell types, under different conditions and with diverse approaches could account in part for the discordant findings.

When IR and IGF-1R are coexpressed, the proreceptors can generate IR–IGF-1R hybrids. These hybrid receptors promote insulin resistance in type II diabetes by decreasing the number of insulin binding sites. A larger fraction of hybrid receptors also increases the number of binding sites for IGF-I and IGF-II and signaling by these growth factors in cancer (Pandini et al., 1999; Benyoucef et al., 2007).

Although several studies point to important biochemical features of the insulin signaling mechanism, few have explored these phenomena at the level of individual cells. We have generated tagged insulin and insulin receptors and used advanced imaging tools to study insulin binding and receptor internalization with a focus on the comparative properties of the two IR isoforms. High-speed optical sectioning confocal and structured illumination microscopy with a programmable array microscope (PAM) (Heintzmann et al., 2001; Hagen et al., 2007) revealed the early steps in ligand-dependent receptor activation and endocytosis. We demonstrated a higher initial rate of internalization of IR-A than IR-B and explored the potential influences on the signaling cascades linked to the IR. It is currently accepted that IR-A is more 'mitogenic' and IR-B more 'metabolic', yet the underlying molecular mechanisms are unclear. We examined certain key points in the insulin pathway: the initial IR activation (autophosphorylation) and ERK activation, a key downstream effector of gene expression. Increased signaling from internalized receptors in endosomes is correlated with increased mitogenicity. In the endosomes, the IR with bound ligand is still activated and can phosphorylate downstream effectors (Di Guglielmo et al., 1994; Pol et al., 1998; Rizzo et al., 2000; Sorkin et al., 2000; Jensen and De Meyts, 2009). Thus, the mitogenic effect of insulin might result from IR signaling from endosomes, whereas the metabolic response of insulin might proceed from IR on the plasma membrane. In view of our microscopy-based evidence for differential internalization, we performed experiments that showed faster endocytosis as well as more persistent and higher activation levels for IR-A than IR-B, reflected in the triggering of the MAPK pathway and ERK1/2 phosphorylation profiles. In addition, IR-A stimulated a higher rate of AP-1 gene transcription whereas IR-B showed higher AKT phosphorylation after insulin stimulation than cells expressing IR-A.

Results

Generation and evaluation of IR constructs

Mammalian expression vectors were generated by fusing IR-A or IR-B to different visible fluorescence proteins (VFPs): eGFP or new variants (Kremers et al., 2006) of CFP (SCFP-3AC) and YFP (SYFP-2F) at the C-terminus of the receptor (IR-GFP, IR-SCFP, IR-SYFP). Specific antibodies against the N-terminus of the IR α-subunit were used in order to evaluate the correct expression and localization of IR-VFPs by immunofluorescence (data not shown). We confirmed correct expression, membrane localization and ligand binding as well as activation, autophosphorylation and internalization after insulin stimulation of the IR chimeras in transfected HeLa cells by microscopy and/or western blots (WBs). After establishing that the transgenes were properly expressed and inserted into the plasma membrane, we determined whether isoforms A and B were colocalized by cotransfecting cells with pcDNA3-IR-A-SCFP and pcDNA3-IR-B-SYFP or with pcDNA3-IR-A-SCFP and pcDNA3-IR-A-SYFP (Fig. 1D,E). Colocalization was quantified by calculation of the Manders coefficient (M) and the Pearson coefficient (Rr). We plotted the product of the differences from the mean (PDM), applying an intensity correlation analysis plug-in (Fig. 1D,E). In addition, frequency scatterplots were computed (Fig. 1D,E). No significant differences in the coefficients for the two pairs were observed. HeLa cells coexpressing IR-A-SCFP and IR-B-SYFP led to Rr=0.90±0.10, M=0.95±0.04, M_{CFP}=0.86±0.04 and M_{YFP}=0.82±0.04 (n=26). In cells coexpressing IR-A-SCFP and IR-A-SYFP, the coefficients were Rr=0.91±0.05, M=0.95±0.04, M_{CFP}=0.87±0.06 and M_{YFP}=0.85±0.04 (n=16).

Biotinamido-caproyl insulin (BAC-Ins) and quantum dots bind to IR and IR-GFP in membranes and filopodia

Biotinylated ligands in combination with streptavidin-conjugated quantum dots (svQDs) provide valuable tools for studying the

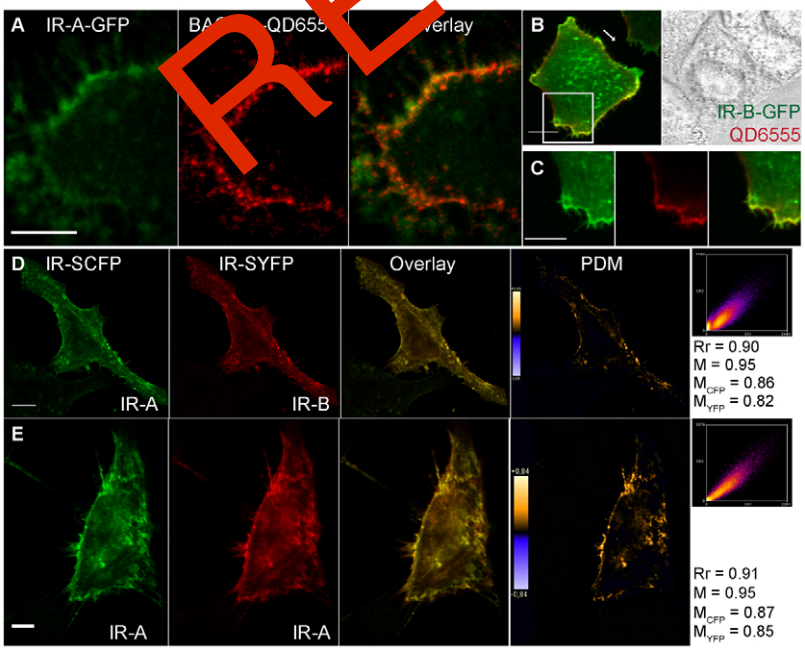

Fig. 1. Imaging of IR in the membrane and filopodia. (**A**) Cells expressing IR-A-GFP, labeled with BAC-Ins and QD655 and imaged live with a programmable array microscope (PAM). Maximum-intensity projections of 25 z-slices with 0.5 µm step size. (**B**) Cells expressing IR-B-GFP, labeled with BAC-Ins and QD655, fixed and imaged by confocal microscopy. Arrow indicates QDs bound to filopodia. (**C**) Zoom of the region inside the square in B. (**D**,**E**) Cells coexpressing IR-A-SCFP and IR-B-SYFP (D) or IR-A-SCFP and IR-A-SYFP (E), labeled in a similar way. PDM graphs and 2D scatterplots of the two intensity distributions are shown (CFP, ordinate; YFP, abscissa). SCFP, green; SYFP, red. Scale bars: 10 µm in A–D; 5 µm in E.

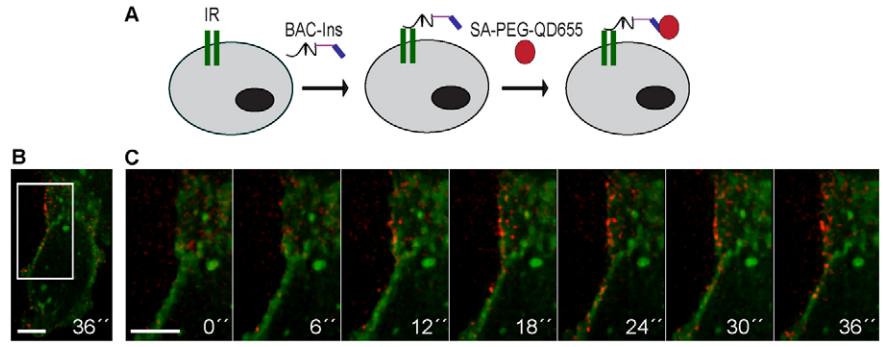

Fig. 2. Binding of QDs in real time. (**A**) Labeling scheme. (**B**) Cell expressing IR-A-GFP labeled with BAC-Ins and 50 pM QD655. QD addition was performed during image acquisition with the PAM at room temperature. See QD binding in real time in supplementary material Movie 1. (**C**) Zoom of region inside the rectangle in B. Maximum-intensity projection of 15 *z*-slices for each time-point with a 50 µm step size. Scale bars: 10 µm.

dynamics of RTKs in living cells, including the characterization of the internalization process and retrograde transport (Lidke et al., 2004; Lidke et al., 2005; Lidke et al., 2007; Cambi et al., 2007; Echarte et al., 2007; Andrews et al., 2009). The combination of the expression of IR-VFPs, binding to the IR of BAC-Ins and its detection with QDs constituted a sensitive monitor of insulin–IR complexes in membranes and on filopodia of HeLa cells. A PAM provided the sensitivity and speed required to visualize individual QDs bound to BAC-Ins and to track them on the plasma membrane and filopodia of living cells expressing IR-A-GFP (Fig. 1A; Fig. 2C). Confocal microscopy was used on fixed cells expressing either IR-B-GFP (Fig. 1B,C) or IR-A-GFP. Binding of QDs was undetectable in the absence of BAC-Ins. For tracking experiments, 50 pM QDs was applied to cells that were exposed to BAC-Ins shortly before QD addition. Fig. 2C shows QD binding during the first 36 seconds after QD addition (supplementary material Movie 1).

Transgenic IR is activated by insulin and its analogs, triggering signaling cascades

HeLa cells expressing IR-GFP (A and B) or IR-B were stimulated over 10 minutes with 100 nM of recombinant human insulin (rhIns) or BAC-Ins after starvation. The activity of the receptors was assayed by immunofluorescence using a specific antibody against phosphorylated IR (Fig. 3A,B; Fig. 4A). Phosphorylated receptor was detected in plasma membranes of IR-A-GFP, IR-B-GFP and IR-B transfected cells, whereas untransfected and non-stimulated cells were negative (Fig. 3A,B; Fig. 4A, respectively). The β-chain was activated in the Golgi of quiescent cells, reflecting the non-assembled receptor. Untransfected cells in the same field served as the controls for non-specific immunostaining (Fig. 3A,B).

The membrane signal reporting activation levels of IR was quantified for IR-A (Fig. 4B). The activation induced by BAC-Ins did not differ within experimental error from the phosphorylation induced by rhIns ($P>0.05$, $n=5–7$; Fig. 4B). In order to evaluate if expression levels had an effect on activation, the ratio between the red (activation level) and green (IR-GFP expression level) signals in the membrane was calculated for each cell. The differences in the activation of the two isoforms were not statistically significant (data not shown).

Western analysis showed that IR and IR-VFPs were equally activated by rhIns (Fig. 3C,D) and by BAC-Ins (Fig. 4C,D). Insulin binding and subsequent IR autophosphorylation trigger mobilization of adaptor proteins (White, 1998; Sebastian et al., 2006). Subsequently, insulin-induced signals propagate through multiple interacting branches, including the MAPK cascade downstream of Ras and the PI3K/AKT pathway (Borisov et al., 2009). Accordingly, we evaluated relevant downstream signaling

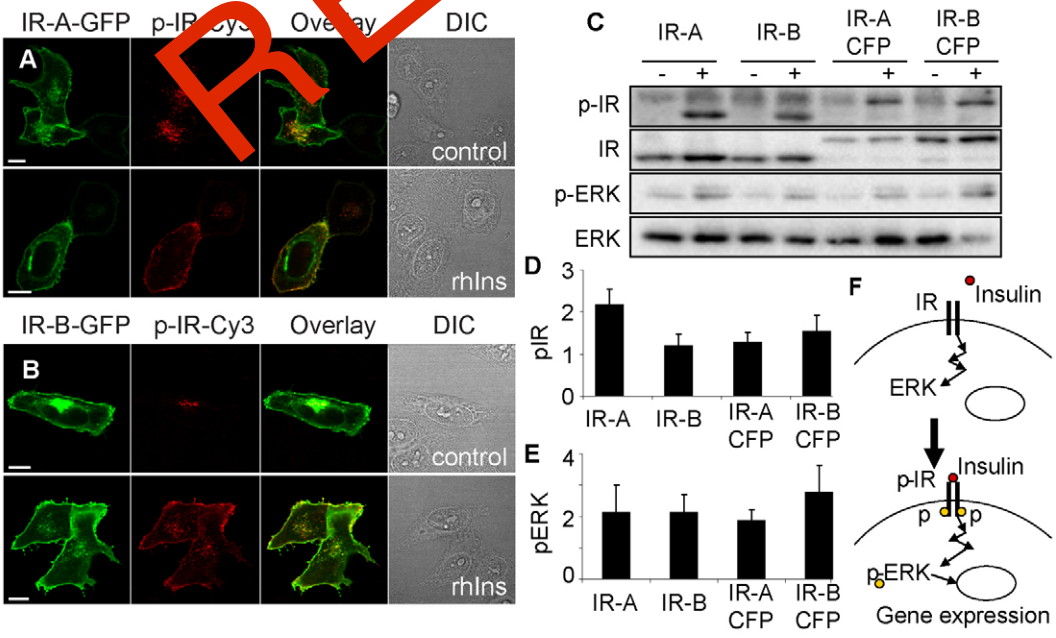

Fig. 3. Expression and activation of IR chimeras by rhIns. (**A**,**B**) Cells expressing IR-A-GFP (A) or IR-B-GFP (B) stimulated (or not) with 100 nM rhIns for 10 minutes, fixed and immunostained for phosphorylated IR. Scale bars: 10 µm. (**C**) Cells expressing IR or IR-CFP stimulated with 100 nM rhIns for 10 minutes and then evaluated by western blot (WB) with anti-PY20, anti-IR, anti-phosphorylated (p44/42) MAPK and anti-ERK. (**D**) Quantification of WB for IR activation. Values for each construct stimulation (+) were normalized with the corresponding value without stimulation (–). The results are shown as the mean + s.d. ($n\geq3$). (**E**) Similar quantification for ERK activation ($n\geq4$). (**F**) Part of the IR signaling pathway. p, phosphorylated forms.

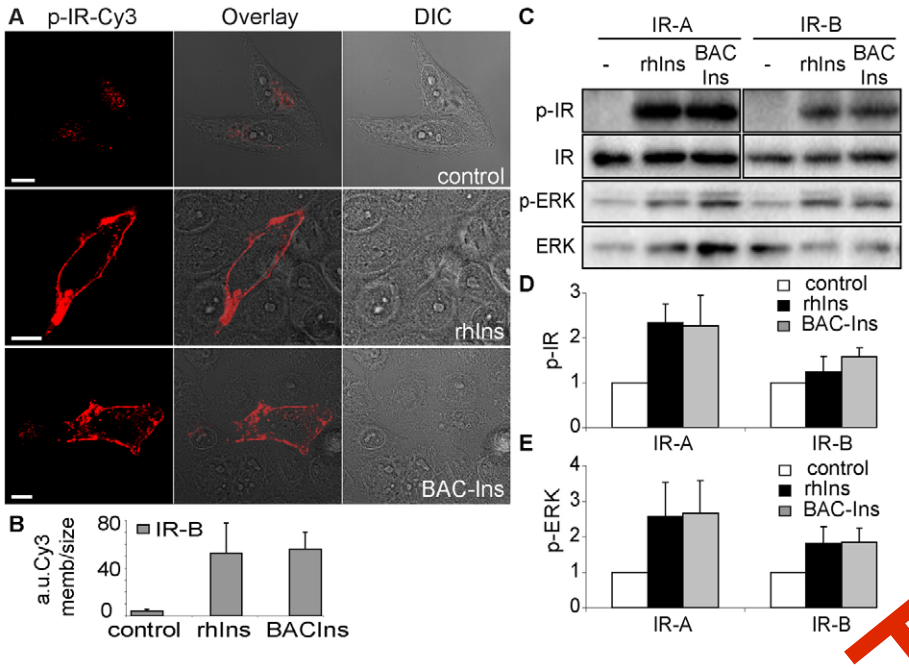

Fig. 4. Activation of IR-A and IR-B by rhIns and BAC-Ins. (**A**) Cells expressing IR-B control or stimulated for 10 minutes with 100 nM rhIns or BAC-Ins, fixed and immunostained for phosphorylated IR. Scale bars: 10 µm. (**B**) Quantification of the phosphorylation signal in the plasma membrane for experiments similar to those shown in A with anti-PY. (**C–E**) WB evaluation of IR and ERK phosphorylation induced by 100 nM rhIns or BAC-Ins for 10 minutes in cells expressing IR-A or IR-B. The results are shown as the mean + s.d. (n=3). p, phosphorylated forms.

events in the IR cascade (Fig. 3F). Activation of ERK1/2 was evaluated by WB in order to test the correct functionality of the chimeras. Cells expressing the different chimeras showed that stimulation by 100 nM rhIns or BAC-Ins triggered ERK1/2 phosphorylation (Fig. 3C,E; Fig. 4C,E).

Visualization of QD–insulin endocytosis

Binding and endocytosis of QD–insulin by IR was assessed by confocal microscopy, before and after short-term acid treatment to remove the acid-labile ligand complex from surface membrane receptors (Haft et al., 1998; Lidke et al., 2004). This procedure demonstrated that the ligand–QD complex was exclusively localized at the plasma membrane after binding and only internalized after subsequent incubation at 37°C.

Cells expressing IR-B, IR-A-GFP and IR-B-GFP were incubated with BAC-Ins followed by QD655, incubated at 37°C and either fixed or treated with acid for 5 minutes before fixation. Confocal microscopy revealed QD binding to the plasma membrane and filopodia at the initial time (0 minutes at 37°C) either in cells expressing IR (supplementary material Fig. S1A,E) or both isoforms of IR-GFP (Fig. 1B,C; Fig. 5A,E), with increasing levels of internalization at later time points of 20, 40 or 150 minutes at 37°C (Fig. 5B,C,E–J; supplementary material Fig. S1B–D,E–H). No significant binding or internalization was detected in untransfected cells, which was as expected because HeLa cells express <5000 endogenous IR per cell (McKeon et al., 1990).

Surface labeling and internalization were recorded by live-cell imaging with a PAM. Before internalization, induction labeling was observed exclusively in the plasma membrane and filopodia. By contrast, QDs were detected inside the cells, colocalizing with GFP after longer incubation periods (Fig. 5K).

The trafficking of BAC-Ins–QD655 was assessed by colocalization with caveolae and early endosomal and lysosomal markers in cells expressing IR-A. At the onset, the BAC-Ins–QD655 complexes colocalized exclusively with caveolin domains in the membrane (supplementary material Fig. S2A). After 20 minutes, the level of colocalization between QD655 and early endosomes increased (supplementary material Fig. S2B,C), whereas at 40 minutes, the QD655 signal was located in perinuclear lysosomes (supplementary material Fig. S2F).

Internalization rate of the insulin–QD complex depends on the expression level of IR

Cells expressing high levels of IR-GFP showed less QD–insulin-IR uptake than cells with lower expression levels. Cells expressing IR-B and exhibiting high levels of QD–ligand binding demonstrated the same tendency. To clarify these observations, cells were classified according to their expression levels: high levels of IR-GFP expression (GFP/cell size >25 cts/pixel) or low levels (GFP/cell size <20 cts/pixel). After 20 and 40 minutes at 37°C, cells with high levels of IR-GFP expression had QDs predominantly on the surface with little internalization (supplementary material Fig. S3A–C). To quantify the effect of expression on insulin-induced internalization, we calculated a ratio between the signal from the BAC-Ins–QD655 complex for the cytosol (QD_i) and that of the plasma membrane (QD_m) plus the cytosol (QD_t=QD_i+QD_m) using image-processing tools on a cell-by-cell basis for both types of cells at different time-points. The differences between the two groups were observed mainly at the initial stage of the endocytosis process. After 20 minutes, cells with low IR-GFP expression levels displayed higher internalization (60±13%, n=13) than cells with high expression levels (35±7%, n=19); the differences were statistically significant (P<0.001; supplementary material Fig. S3D). The effects of receptor abundance decreased with incubation time, leading to smaller differences between the two groups at 40 minutes (high expression, 62±13%, n=8; low expression, 71±13%, n=18) and 150 minutes (high expression, 90±6%, n=14; low expression, 92±4%, n=8).

IR-A internalizes more readily than IR-B

The series of images acquired during internalization allowed a quantification of QD endocytosis on a cell-by-cell basis, comparing the behavior of each IR isoform. We performed the same type of analysis as described above on cells expressing IR-B, quantifying QD internalization after 20 minutes (48%±7%, n=17), 40 minutes

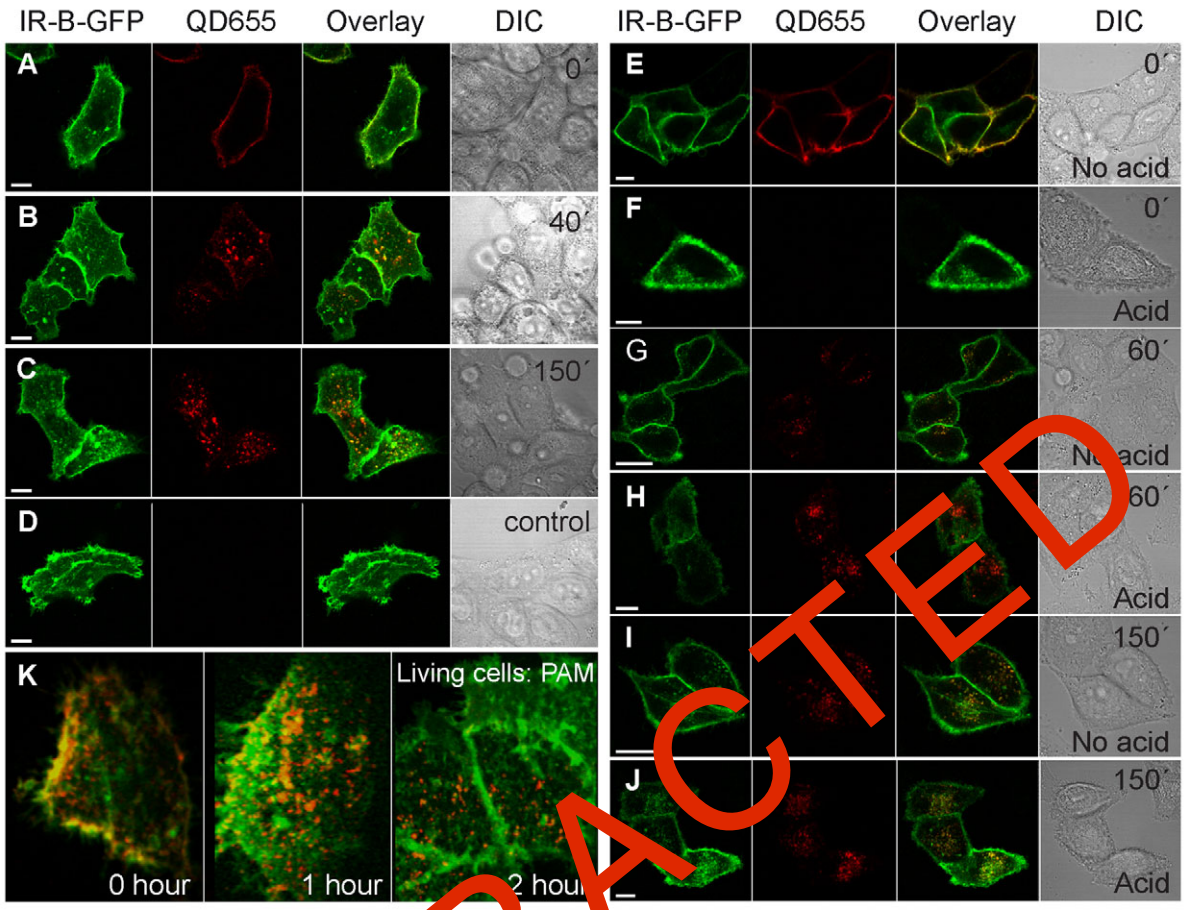

Fig. 5. Labeling and internalization of IR-GFP. Cells expressing IR-B-GFP were labeled in vivo with BAC-Ins and QD655. (**A**–**C**) Cells were incubated at 37°C for the indicated times and fixed. (**D**) Non-specific QD binding control. Cells were incubated only with QD655 without previous exposure to BAC-Ins. (**E**,**G**,**I**) Cells were incubated at 37°C for 0, 60 or 150 minutes, respectively, and directly fixed without any other treatment. (**F**,**H**,**J**) Cells were exposed to acid before fixation. (**K**) 3D reconstruction of labeled cell expressing IR-B-GFP, incubated for 0, 1 or 2 hours at 37°C and imaged live with a PAM. Scale bars: 10 µm.

(64%±18%, *n*=39) and 150 minutes (81%±10%, *n*=23). Internalization rates at each time-point were significantly different ($P<0.001$; Fig. 6B), defining a distinctive temporal pattern. We tested these results using fluorescent bovine insulin (FITC-Ins), performing similar experiments but in a single step. Quantification of FITC-Ins internalization (20 minutes: 46%±5%, *n*=12; 40 minutes: 60%±14%, *n*=12; and 150 minutes: 75%±12%, *n*=15) showed no significant differences to that of the BAC-Ins–QD655 internalization (Fig. 6B). These results demonstrate that QD did not interfere with the endocytosis process and provided the advantage of a stronger, more stable signal.

No significant differences were found in QD internalization in cells expressing IR-B or IR-B-GFP at 20 minutes (44±14%, *n*=21), 40 minutes (67±13%, *n*=22) or 150 minutes (87±8%, *n*=9) (Fig. 6C). We conclude that VFPs did not affect the uptake of insulin.

Next, we compared the internalization of both isoforms. At early times (20 minutes), the analysis demonstrated a higher rate of internalization for IR-A-GFP (65±11%, *n*=10) than for IR-B-GFP (47±13%, *n*=16; Fig. 6D). These differences were statistically significant ($P\leq0.001$). However, at longer incubation periods [40 minutes (IR-A-GFP: 77±16%, *n*=3; IR-B-GFP: 70±12%, *n*=17); 150 minutes (IR-A-GFP: 92±3%, *n*=5; IR-B-GFP: 87±10%, *n*=6)], the differences were no longer significant, although there was a higher tendency for IR-A internalization.

Differential activation of IR isoforms induced by insulin

The differences observed in the rate of internalization of the receptor isoforms prompted an investigation of downstream signaling. We measured IR phosphorylation after ligand binding. WB experiments were performed with cells expressing IR-A, IR-B or both together, stimulated with 50 nM rhIns for 2, 5 or 15 minutes (Fig. 7A,B). IR-A showed higher and sustained activation levels than cells expressing IR-B or both isoforms together (fold-induction at 2, 5 and 15 minutes, respectively: for IR-A, 1.8±0.4, 1.6±0.3, 1.8±0.4; for IR-B, 1.5±0.3, 1.3±0.4, 1.2±0.2; for both isoforms, 1.6±0.3, 1.3±0.3, 1.1±0.3). Activation of IR after 15 minutes was statistically different ($P\leq0.05$) for cells expressing IR-A ($n\geq4$).

IR-A induced ERK1/2 activation more rapidly and sustained the activation longer than IR-B

To evaluate the signaling of the IR cascade further downstream, we assayed ERK1/2 phosphorylation. Cells expressing IR-B showed a clear maximum of ERK1/2 activation after 5 minutes of stimulation (fold-induction: 2.4±0.7 at 5 minutes, 1.8±0.6 at 2 minutes and 1.3±0.4 at 15 minutes), whereas activation in cells expressing IR-A peaked earlier: 2.7±0.8-fold at 2 minutes and 2.7±1.5-fold at 5 minutes. In the case of coexpression of both receptors, the temporal profile of activation was similar to that of

Journal of Cell Science

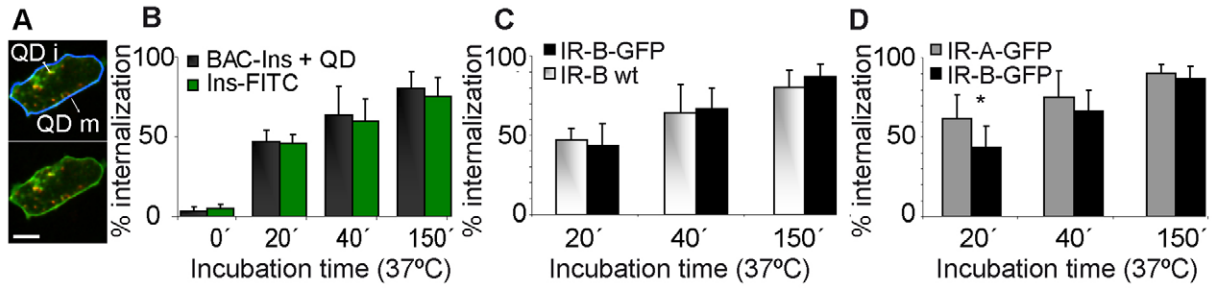

Fig. 6. IR-A internalizes more readily than IR-B. (**A**) Segmentation of the membrane. (**B**) Cell-by-cell quantification of internalized IR-B–BAC-Ins–QD655 using Matlab or similar quantification of internalized IR-B–FITC-Ins. (**C**) Comparison between IR-B and IR-B-GFP internalization. (**D**) Comparison between IR-A-GFP and IR-B-GFP internalization [low receptor expression levels (GFP/size cell <30 cts/pixel)]. The asterisk shows significant differences ($P \leq 0.001$). Results are shown as the mean + s.d.

IR-B alone, although the maximal activation was somewhat higher (2.9±0.9 at 5 minutes; $P<0.05$) than with either isoform alone. These results demonstrate that ERK1/2 activation occurs more rapidly and is sustained longer upon stimulation of IR-A (Fig. 7C–E).

Stimulation of AP-1 gene transcription is higher for IR-A than for IR-B

MAPK activation state is crucial for AP-1-dependent gene expression (Pastore et al., 2005). To evaluate the downstream relevance of the differences detected between IR isoforms, we measured AP-1 gene transcription using a reporter gene. The AP-1-dependent reporter plasmid (AP-1-luc), containing seven tandem copies of the AP-1 site, was used to transfect cells in combination with pcDNA3-IR-A, pcDNA3-IR-B or the empty vector (EV). Induction of luciferase activity was measured after 16 hours of stimulation with 100 nM rhIns in each case (Fig. 7F). AP-1 activity was higher when stimulating IR-A than IR-B and the difference was statistically significant ($P=0.004$, $n=6$).

AKT activation is differentially induced by IR isoforms

The next step was to evaluate the activation of the metabolic pathway by IR, which regulates and maintains glucose homeostasis in response to insulin (Fig. 7J). AKT activation was measured by phosphorylation of serine 473 in cells coexpressing AKT fused with the HA epitope (AKT-HA) and either IR-A, IR-B or EV, stimulated with 100 nM rhIns. IR-B induced a higher AKT phosphorylation than IR-A (fold-induction at 2, 5 and 15 minutes: for IR-B, 5.8±2.3, 6.8±0.9, 5.1±2.1; for IR-A, 4.1±1.4, 4.1±0.5, 3.3±1.1). The differences were statistically significant for 5 minutes ($P<0.001$, $n=5$; Fig. 7G,H). In addition, AKT activation was monitored by wide-field microscopy in cells coexpressing AKT-HA and either IR-A or IR-B and stimulated or not (control) with 100 nM rhIns over 5 minutes at 37°C. These results were consistent with those of the previous WBs (Fig. 7I).

Colocalization of IR-GFP and insulin–QD decreases after endocytosis

To evaluate the ligand-receptor complex and its dissociation after internalization, we analyzed the colocalization of BAC-Ins–QDs bound to IR-GFP over time. At the onset of endocytosis, BAC-Ins–QDs localized at the cell surface (Fig. 8A), redistributing later to the perinuclear region (Fig. 8B). We evaluated colocalization across the cell body by superimposing the two signals over linear trajectories (Fig. 8D). After 1 hour, BAC-Ins–QD655–IR-GFP complexes colocalized in endosomes (Fig. 8H).

To quantify colocalization using Manders coefficients, cells were classified into four groups based on the extent of the endocytosis: S0–S3 (Fig. 8H). The analysis of M revealed differences between S0 (0.90±0.03) and both S2 (0.73±0.05) and S3 (0.79±0.07), with a $P<0.001$. Significant differences were also observed between S1 (0.86±0.05) and S3 (0.79±0.07; $P<0.05$). S0 and S1 showed no significant differences in their colocalization coefficients (Fig. 8G).

Manders maps showed the contribution of each pixel to the global M. At the onset of endocytosis, higher contributions were in the membrane but this contribution disappeared in S3 cells, leading to maximum contributions at perinuclear regions (Fig. 8H). At intermediate steps, colocalization persisted in the membrane but there were other loci of association, probably in early endosomes. At S3, colocalization was low, indicative of a dissociation of the complexes in late endosomes or lysosomes (Fig. 8H).

Discussion

Generation of the mammalian expression vectors with IR-A and IR-B fused to eGFP, SCFP or SYFP in combination with biotinylated insulin and QDs allowed the direct visualization of ligand-bound and activated IR in membranes and filopodia of living cells. Quantitative imaging provided a tool for studying the early steps of endocytosis of receptor-ligand complexes in a novel way. Coexpression of both isoforms fused to different VFPs revealed colocalization of IR-A and IR-B. The *M* and *Rr* coefficients were similar to those calculated when the same isoform was coexpressed fused to the VFPs SCFP and SYFP. These results are in agreement with previous reports demonstrating (or assuming) the existence of IR-A and IR-B heterodimers (Pandini et al., 1999; Benyoucef et al., 2007; Blanquart et al., 2008). By contrast, Uhles et al. (Uhles et al., 2003) reported experiments on pancreatic beta cells using fluorescence resonance energy transfer, according to which IR isoforms localized to different membrane domains, abrogating the formation of heterodimers and promoting isoform-specific IR signaling.

Cells incubated with the preformed BAC-Ins–QD655 complex (formed with different BAC-Ins:QD655 ratios) showed no labeling. By contrast, biotin insulin (lacking a tether) bound to cells was recognized by fluorescent streptavidin but not by QDs, probably owing to steric hindrance. These results are consistent with the binding model proposed by Ward et al. (Ward et al., 2007).

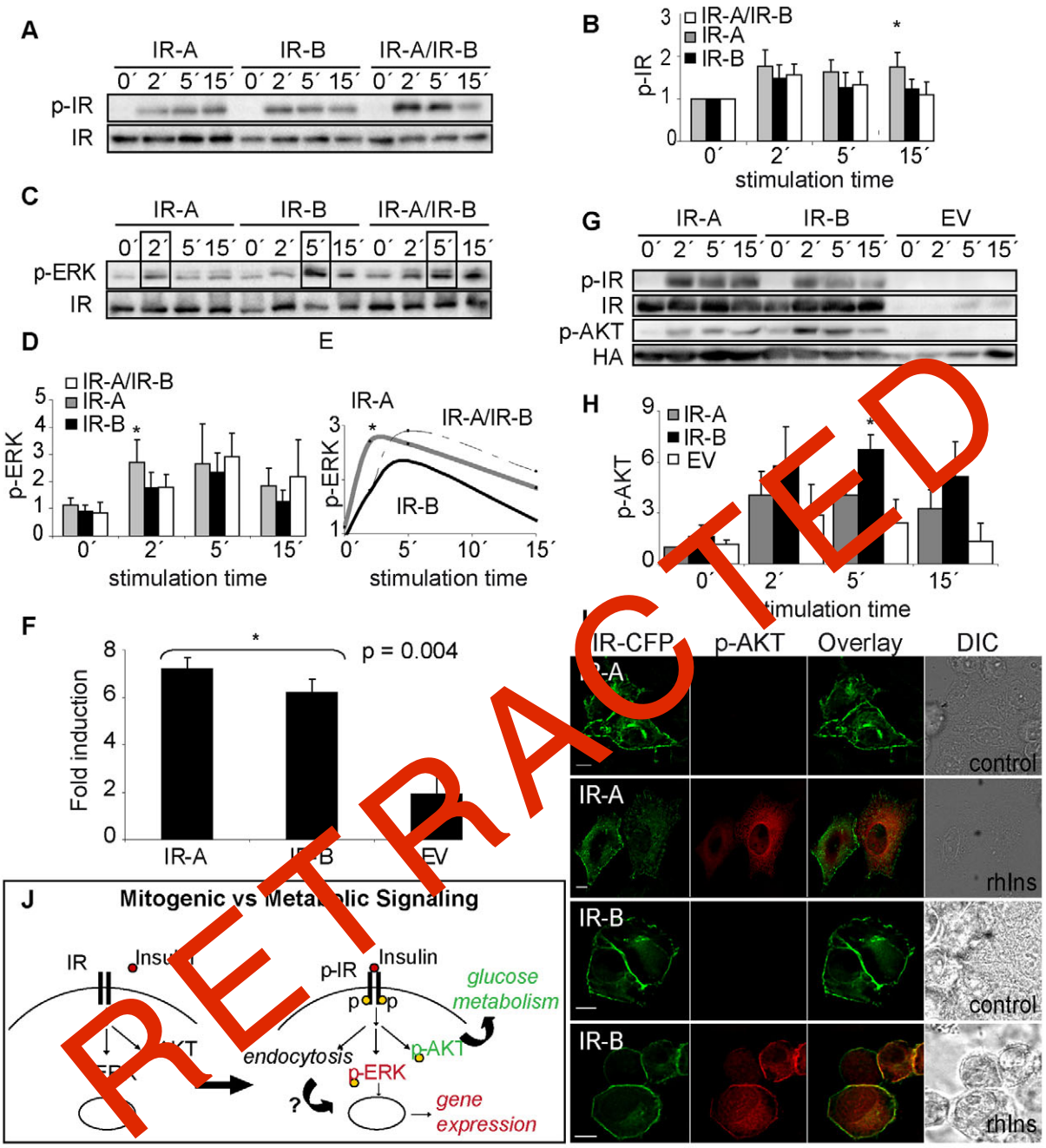

Fig. 7. Differential signaling pathway of IR-A and IR-B. (**A**,**C**) Activation profiles of IR and ERK. Cells expressing IR-A, IR-B or both together were stimulated with 50 nM rhIns for different times (2, 5 and 15 minutes) and analyzed by WB with anti-PY20 and anti-IR (A) or anti-phosphorylated (p44/42) MAPK and anti-ERK (C). (**B**,**D**,**E**) Quantitative results of WBs are shown in B (phosphorylated IR), D and E (phosphorylated ERK; the phosphorylated ERK signal was normalized by the mean of the unstimulated controls of each experiment). The results are shown as the mean + s.d. ($n \geq 4$ for IR experiments and $n \geq 6$ for ERK experiments). (**F**) HeLa cells coexpressing AP-1-luc and IR-A, IR-B or EV. Luciferase activity was measured and the fold-induction was calculated ($n=6$ experiments). (**G**) AKT phosphorylation (Ser473) profiles in cells coexpressing AKT-HA and IR-A or IR-B or EV, starved for 16 hours and stimulated with 100 nM rhIns for different times (2, 5 and 15 minutes). (**H**) Quantification of AKT activation performed as for ERK experiments. The results are shown as the mean + s.d. ($n \geq 5$). Asterisks in B, D–F and H indicate significant differences ($P<0.05$) (**I**) Immunofluorescence experiments by wide-field microscopy showing AKT phosphorylation. Deconvolved middle frame of 80 *z*-stacks with 0.2 µm step size. Scale bars: 10 µm. (**J**) Mitogenic versus metabolic signaling scheme of the IR pathway. p, phosphorylated forms.

Either rhIns or BAC-Ins induced receptor autophosphorylation in the membrane, a hallmark of insulin activity. We also observed receptor autophosphorylation in the ER and the Golgi both in starved transfected cells and after insulin addition, probably owing to the inherent activity of the β-subunit prior to IR assembly and dimerization (Patti and Kahn, 1998). BAC-Ins not only induced IR autophosphorylation but also triggered the insulin signaling cascade as revealed by ERK1/2 and AKT activation.

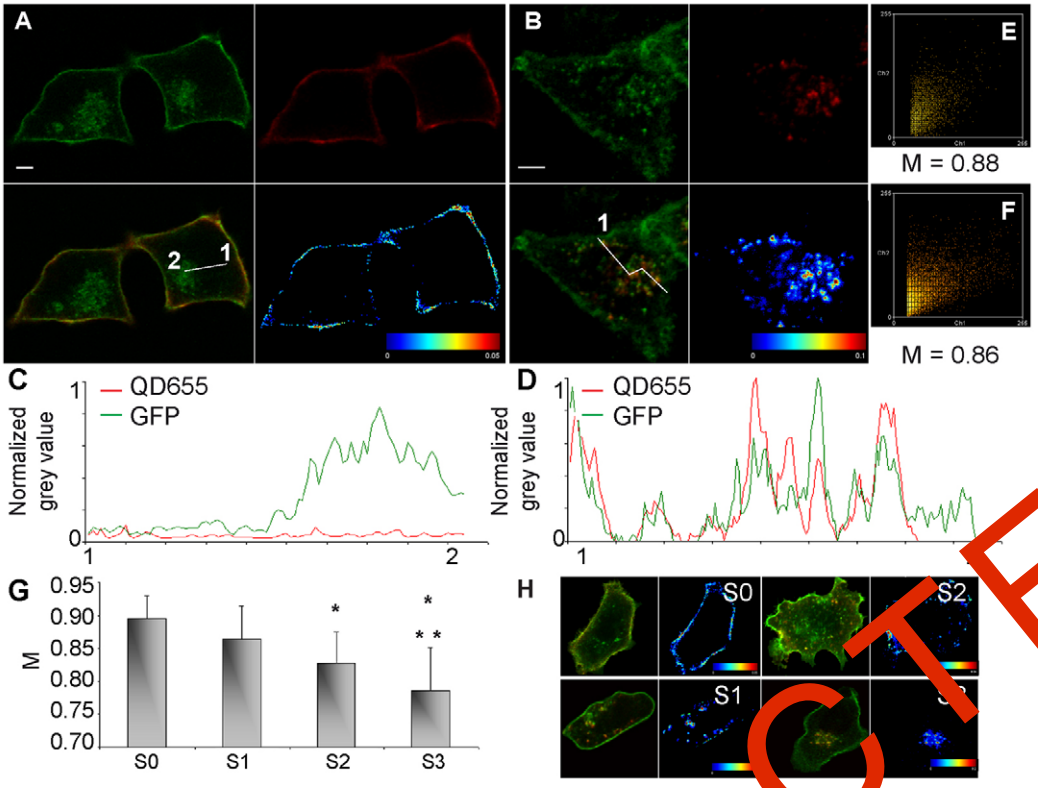

Fig. 8. Colocalization during the endocytosis process. (**A**,**B**) Cells expressing IR-B-GFP and labeled with BAC-Ins and QD655, without induction of internalization (A) or after 1 hour at 37°C (B) were fixed and imaged by confocal microscopy. (**C**,**D**) Linear trajectories crossing the cell of the two signals using Image J. All signals were normalized by the maximum (C corresponds to line shown in A; D corresponds to line shown in B). (**E**,**F**) Frequency scatter plot of one slice performed with the ImageJ intensity correlation analysis plug-in (channel 1, QD channel; channel 2, GFP). (**G**) Manders coefficient for each group of cells. Asterisks indicate a significant difference with S0 ($P<0.001$). Double asterisks indicate significant differences with S1 ($P<0.05$). (**H**) Examples of cells according to the performed classification (overlay between QD signal and GFP signal and Manders maps are shown).

The endocytosed IR-insulin complex visualized at different time-points appeared at the plasma membrane, in endosomes close to the membrane or in perinuclear regions. In the latter case, the insulin-IR complexes dissociated.

Cell-by-cell analysis revealed that high level of IR-GFP expression led to a slower rate of internalization compared with cells with low expression, a result not attainable from previous studies based on biochemical and radiolabeled ligand determinations of bulk cell populations. We quantified the internalization properties of each IR isoform and demonstrated a higher initial rate of internalization of IR-A-GFP than IR-B-GFP, concordant with other reports using different experimental approaches (Vogt et al., 1991; Yamaguchi et al., 1991). It is possible that the differences between the endocytic properties of the two IR variants are tissue-specific and potentially important in the regulation of IR recycling or downregulation in vivo.

Impaired receptor internalization has been described in mutants affecting the autophosphorylation (Reynet et al., 1990; Wilden et al., 1990) or altering the intracellular β-subunit, in particular the juxtamembrane region (Backer et al., 1990; Thies et al., 1990) or ATP binding site (McClain, 1987; Hari and Roth, 1987; Russell et al., 1987; Yamamoto et al., 1990). The differences in the rate of internalization of the two IR splicing variants raise the question as to whether the phenomenon could be influencing other steps of the signaling pathway. In view of the well-accepted view that IR-A is more mitogenic than IR-B, we evaluated three points of this pathway: the initial step (IR autophosphorylation), an intermediate step (ERK1/2 phosphorylation) and a late mitogenic effect (gene transcription via AP-1). We observed that IR-A showed a greater and more persistent activation than IR-B, although cells coexpressing both isoforms also showed high activation, albeit more transient in nature. With respect to ERK1/2 activation, there were significant differences consistent with differential endocytosis. Whereas IR-B-induced ERK1/2 activation peaked at 5 minutes, IR-A led to more activation at 2 minutes than the B isoform. The differences between the signals after 2 minutes and 5 minutes of stimulation were larger in the case of cells coexpressing IR-A and IR-B. In endosomes, ligand-bound IR can still phosphorylate downstream effectors (Sorkin et al., 1993; Di Guglielmo et al., 1994; Bergeron et al., 1995; Grimes et al., 1996; Pol et al., 1998; Rizzo et al., 2000; Sorkin et al., 2000), prompting the hypothesis that the mitogenic effect of insulin might originate from IR signaling from endosomes.

In addition, blocking IR internalization led to inhibition of SHC phosphorylation and activation, whereas no effect was detected on IR autophosphorylation or IRS1 and AKT kinase phosphorylation and activation (Biener et al., 1996; Ceresa et al., 1998; Hamer et al., 2002), suggesting that these signaling elements can be fully activated by IRs at the surface. That is, the metabolic response of insulin appears to be fully activated from IRs on the cell surface. Our results are consistent with these interpretations: the isoform (IR-A) that is activated in a higher and more persistent manner (measured as receptor autophosphorylation) by insulin internalizes more readily, triggering the mitogenic pathway and inducing the ERK1/2 cascade earlier and stimulating gene transcription through the AP-1 pathway to a greater degree. By contrast, IR-B internalization is slower, allowing greater signaling from the membrane via AKT activation, an important step in the regulation of glucose metabolism. In conclusion, we identify the internalization dynamics as a (the) possible mechanism responsible for the differential signaling of the two splice variants of IR.

Materials and Methods

Materials

The rhIns was kindly provided by Laboratorios Beta (Buenos Aires, Argentina). Bovine BAC-Ins and FITC-Ins were from Sigma. Monoclonal mouse anti-PY99, polyclonal rabbit anti-ERK2 and polyclonal rabbit anti-AKT-*P* (Ser473, for WBs)

were from Santa Cruz Biotechnology (Paso Robles, CA). Monoclonal rabbit anti-(phosphorylated IR-β-subunit) (Tyr1361), monoclonal mouse anti-IR-β-subunit, polyclonal rabbit anti-phosphorylated (p42/44) MAPK and monoclonal rabbit anti-AKT-*P* (Ser473, for immunofluorescences) were from Cell Signaling Technology. Anti-HA was from Covance (Emeryville, CA). The QD655 conjugated with streptavidin was from Invitrogen. Anti-CD63 (rabbit) was from Santa Cruz. Caveolae and EEA1 markers (rabbit) were from Abcam (Cambridge, UK).

The pCMV-AKT-HA vector was provided by Anabella Srebrow, Laboratorio de Fisiología y Biología Molecular (LFBM), FCEN, UBA, Argentina. The pCMV-β-galactosidase and the plasmid containing luciferase reporter gene downstream of seven binding sites for AP-1 were provided by Omar Coso (LFBM).

Expression constructs

IR-A and *IR-B*: cDNA of *IR-A* or *IR-B* were provided by Axel Ullrich (MPIbpc, Germany) and amplified by PCR using primers containing the *Hin*dIII restriction site (IR forward: 5′-aagcttatggccaccgggggccgg-3′) and *Nhe*I and *Xba*I sites (IR reverse: 5′-tctagagctagcgaaggattggaccgaggcaaggtc-3′). The products were digested with *Hin*dIII and *Xba*I enzymes and cloned into the pcDNA3 vector.

IR-GFP, *IR-SCFP* and *IR-SYFP*: peGFP-C3 (Clontech) or pSCFP-3AC or pSYFP-2F (provided by T. W. Gadella Jr, University of Amsterdam, The Netherlands) were digested with *Nhe*I and *Apa*I and cloned into pcDNA3-IR-A and pcDNA3-IR-B.

Cell culture and transfections

Cell culture reagents [Dulbecco's modified Eagle's medium (DMEM), Glutamax, Optimem and FBS] were from Gibco (Grand Island, NE). HeLa cells were maintained in DMEM supplemented with penicillin, streptomycin and 10% FBS at 37°C in 5% CO_2.

HeLa cells were plated at 1×10^5 cells per well in 24-well plates and onto 12 mm glass coverslips (microscopy) or at 2.5×10^5 cells per well in 12-well plates (WBs) 1 day before transfection in DMEM and 10% FBS without antibiotics. Cells were transfected with Lipofectamine Reagent 2000 (Invitrogen, Carlsbad, CA) over 5 hours. After transfection, cells were cultured for further expression in complete medium. For AKT experiments, we used 0.2 µg AKT-HA and 0.6 µg IR per well.

Western blots

Following stimulation with 50 nM rhIns (stimulation profiles experiments for 2, or 15 minutes) or 100 nM rhIns or BAC-Ins (other experiments for 10 minutes), cells were lysed in buffer containing 50 mM Tris-HCl, pH 7.5, 1 mM EDTA, 1 mM EGTA, 150 mM NaCl, 10% glycerol, 1% NP40, 1 mM $MgCl_2$, 0.1% SDS, 2 mM Na_3VO_4, 40 mM sodium β-glycerophosphate, 1 mM DTT, 1 mM NaF and a protease inhibitor cocktail (Roche) and centrifuged for 10 minutes at 12,000 ***g*** at 4°C. The supernatants were mixed with loading loading buffer (50 mM Tris-HCl, pH 6.8, 2% SDS, 0.1% Bromophenol Blue, 10% glycerol and 100 mM β-mercaptoethanol) and heated for 5 minutes at 100°C. Following 10% SDS-PAGE and transfer, membranes were blocked in 5% w/v non-fat dried milk in 0.1% Tween-TBS buffer (TTBS) for 1 hour, washed and incubated overnight at 4°C with primary antibodies diluted in 5% BSA in TTBS [anti-IR β-subunit, 1/500; anti-ERK, 0.4 µg/ml; anti-phosphorylated (p44/42) MAPK, 1:500; anti-HA, 1:1000] or in 2% BSA in TTBS (anti-PY20, 2 µg/ml; anti-AKT-*P*, 0.4 µg/ml). The following day, membranes were incubated with secondary antibodies for 1 hour and washed. The blots were developed by chemiluminescence using a Bio-Imaging Analyzer Fujifilm LAS-1800 II and Image Gauge 3.12, Fujifilm (FCEN, UBA, Argentina). Quantification was performed using Image J (NIH), measuring the optical density of the blotted membrane bands. For IR experiments, values for stimulated samples were normalized with the corresponding value without stimulation and this was indicated as fold-induction. For ERK and AKT phosphorylation, the signals were normalized by an average of signals from unstimulated cells. In all the experiments, we controlled loading with the total blotting (IR, ERK and HA.AKT) because all of the samples were from an equal initial number of cells. The results were expressed as the mean of at least three independent experiments (±s.e.m.). *P* values were estimated using two-tailed Student's *t*-tests.

Luciferase reporter assay

Cells seeded onto 12-well plates (2×10^5 cells/well) the day before were transfected using 0.6 µg pcDNA3-IR or EV, 0.1 µg AP-1-luc and 0.1 µg pCMV-β-galactosidase (transfection control). After 24 hours, cells were starved for one day and then stimulated with 100 nM rhIns over 16 hours. Luciferase activity was determined using luciferase reactive and reporter lysis buffer (Promega, Madison, WI) and normalization to the control (non-stimulated cells) was performed (fold-induction). Protein concentration and β-galactosidase activity were measured as controls. The results were expressed as the mean of at least three independent experiments (± s.e.m.).

Labeling in vivo with QDs and BAC-Ins or FITC-Ins and internalization

Before the experiment, cells expressing IR-B, IR-A-GFP or IR-B-GFP and starved overnight were washed with Tyrode's buffer at room temperature (RT) and incubated with 50 nM BAC-Ins or FITC-Ins for 15 minutes at 15°C or RT, washed with Tyrode's buffer and incubated with 50 pM or 1 nM QD655 (in the case of BAC-Ins) depending on the experiment for 10 minutes at 15°C or RT, and washed and either fixed in 3.7% PFA on ice for 20 minutes or incubated at 37°C for different periods of time before fixation. When acid treatment was applied, cells were incubated for 5 minutes at RT with 0.1 M Na-glycine, pH 3 and 0.5 M NaCl.

IR and AKT activation by immunofluorescence

After overnight starvation, transfected cells were stimulated with 100 nM rhIns or BAC-Ins for 10 minutes (IR activation) or with 100 nM rhIns for 5 minutes (AKT activation), washed with PBS and immediately fixed in cold methanol for 30 minutes at –20°C, blocked with PBS with 0.3% Triton X-100 and 1% BSA for 1 hour at 37°C and incubated with antibodies against phosphorylated IR-β-subunit (0.3 µg/ml), PY99 (1 µg/ml) or AKT-*P* (1/1000) overnight at 4°C. The following day, samples were incubated with a secondary antibody conjugated to Cy3 or Alexa Fluor 555 for 1 hour at 37°C and washed. IR activation was monitored by confocal microscopy and AKT activation by wide-field microscopy.

In vivo PAM experiments

Cells expressing IR-A-GFP were starved overnight and labeled as we described. For imaging of QD binding, the cells were incubated with 50 pM QD655 during image acquisition. For internalization experiments, we used 1 nM QD655 at RT.

Microscopy

Confocal laser scanning microscopy was performed with a Zeiss LSM 510 Meta System using a C-Apochromat 63× 1.2 NA water immersion objective or a Plan-Apochromat 63× 1.4 NA oil-immersion objective. Excitation and filters were as follows: GFP, argon ion excitation 488 nm, emission 505–520 nm BP filter; QD655, excitation 488 nm and 458 nm, emission >650 nm; Cy3, DSSP laser excitation 532 nm, emission 563–606 nm BP filter.

For experiments with IR-SCFP and IR-SYFP and assays with endocytosis markers, a confocal Olympus FluoView FV1000 microscope was used with a PLSAPO 60× 1.35 NA oil-immersion objective and a UPLSAPO 60× 1.2 NA water-immersion objective. Excitation and emission filters were as follows: CFP, excitation 458 nm, emission 475/25 nm filter; YFP, excitation 515 nm, emission 530/10 nm BP filter; Alexa555, excitation 543 nm; emission 560–620 nm BP filter; QD655, excitation 405 nm; emission 655–685 nm BP filter.

Wide-field microscopy for AKT experiments was performed with an Olympus IX71 microscope using a 40× 1.15 NA water-immersion objective, with mercury vapor lamp excitation and filters suitable for CFP and Alexa555. The camera used was a Hamamatsu Orca CCD C4742-95.

PAM experiments were performed with an LCoS-based system (Hagen et al., 2009) with the following parameters: light source, argon ion 488 nm; sensor, Andor emCCD camera, Ixon DV897-BV, 512×512 pixels, –87°C; exposure, 16 milliseconds, 4× average (for some internalization experiments) and 50 milliseconds, single exposure (for QD binding experiments and some internalization experiments); objective, 60× 1.2 NA water immersion; images, 158 nm/pixel in *xy*, 0.5 µm *z*-optical sections; filters, GFP – 525/50 nm BP, QD – 655/40 nm BP.

Image processing

Confocal microscope and PAM images were processed with Matlab and Image J. In confocal images, the background of each channel (median or mean of empty region) was subtracted and, in some cases, a median filter was applied (radius: 1 pixel) only for presentation. No filter was applied in quantitative analyses.

In the first PAM image (Fig. 1A), we made a maximum-intensity projection from a stack of images after removing the background and applying thresholds for GFP (GFP>40 cts) and QD (GFP>600 cts) signals only for presentation. QD images were multiplied by a factor of two and a median filter (radius: 1 pixel) was applied to the GFP image. The latter was corrected for photobleaching by normalizing the signal of each frame to its maximum value before taking the maximal intensity projection from the stacks. 3D reconstruction of PAM images was performed with Matlab and the Image J plug-in.

Wide-field images were processed with Image J for presentation; the background of each channel, evaluated in regions lacking cells, was subtracted from each foreground value. The *z*-stacks (80 frames, 0.2 µm step size) were deconvolved using Huygens Professional Scientific Volume Imaging version 3.6 software, applying a quick maximum likelihood estimation algorithm (QMLE).

Colocalization analysis during endocytosis

Cells were classified according to the stage of endocytosis: S0 (internalization not induced and QD signal at the plasma membrane); S1 (QD signal detected very close to the membrane); S2 (more internal red signals but QDs not already in the perinuclear region); and S3 (QD signal predominantly in perinuclear regions).

Colocalization during endocytosis was analyzed by introducing a new mask defined as the pixels for which the QD signal was >2× the mean of the QD signal in the entire cell mask. After that, the Manders coefficient was calculated as described (only cells with a mean GFP signal >500 cts and <5500 cts were considered).

Internalization analysis

For quantitative internalization experiments, labeling was done at 15°C to minimize endocytosis. We defined $t=0$ as the end of labeling washings and $t=20$, 40 and 150 minutes were periods of incubation at 37°C.

Segmentation (membrane and interior)

Channel backgrounds (median) were subtracted. In QD images, bleed-through contributions were subtracted. Segmentation was performed for each cell using the GFP signal (IR-GFP experiments) or differential interference contrast (DIC) images (IR wild-type experiments). After cell segmentation, the pre-membrane was defined as the difference between the image of the cell and a binary erosion (iterations: 5–20; alternating connectivity); we evaluated the results visually. The pre-interior was defined as the difference between the cell and the pre-membrane. A QD_{mask} was marked by red pixels. With this mask, the membrane was defined as the product of the QD_{mask} and the pre-membrane, and the interior was defined as the product of the QD_{mask} and pre-interior obtained previously.

Estimation of the relative amount of internalization

Values in the membrane and the interior were summed for the red and green channels and sizes were also measured. To compute the relative amount of internalized red fluorescence, we estimated QD_{total} (QD_t) as the sum of $QD_{membrane}$ (QD_m) and $QD_{interior}$ (QD_i) and calculated for each cell the ratio QD_i/QD_t. This 'internal calibration' approach was chosen to remove the influence of the amplifier gain and the zoom factor for each image acquisition condition. The expression levels were estimated as the mean of the GFP signal (sum of GFP divided by cell size). The equivalent procedure was applied to images based on fluorescein signals.

Endocytosis immunofluorescence

HeLa cells expressing IR-A were labeled with BAC-Ins and QD655, internalization was induced and then cells were fixed in PFA. Immunofluorescence experiments were performed with 6 μg/ml caveolae marker, 4 μg/ml anti-CD63 and 1.5 μg/ml EEA1.

Colocalization analysis

IR-A-SCFP with IR-B-SYFP and IR-A-SCFP with IR-A-SYFP

Rr, M, M_{CFP} and M_{YFP} were calculated with Matlab as follows after background subtraction, and cell segmentation was performed manually:

$$Rr = \frac{\sum (Im_{CFP} - \overline{Im_{CFP}}) \times (Im_{YFP} - \overline{Im_{YFP}})}{\sqrt{\sum (Im_{CFP} - \overline{Im_{CFP}})^2 \times \sum (Im_{YFP} - \overline{Im_{YFP}})^2}}, \quad (1)$$

$$M = \frac{\sum (Im_{CFP} \times Im_{YFP})}{\sqrt{\sum (Im_{CFP})^2 \times \sum (Im_{YFP})^2}}, \quad (2)$$

$$M_{CFP} = \frac{\sum_i Im_{CFPicoloc}}{\sum_i Im_{CFPi}}, \quad (3)$$

$$M_{YFP} = \frac{\sum_i Im_{YFPicoloc}}{\sum_i Im_{YFPi}}, \quad (4)$$

where Im_{CFP} is the image from CFP channel, Im_{YFP} is the image from YFP channel and $Im_{CFPicoloc}$ and $Im_{YFPicoloc}$ are the colocalized pixels in Im_{CFP} and Im_{YFP}. For M_{CFP} and M_{YFP}, pixels with intensity higher than half of the mean of CFP and YFP signal were considered as colocalized pixels. The PDM graph was generated using an intensity correlation analysis plugin (Image J). For each pixel:

$$PDM = (Im_{CFP} - \overline{Im_{CFP}}) \times (Im_{YFP} - \overline{Im_{YFP}}). \quad (5)$$

The frequency scatterplot was performed by applying a plug-in of Image J.

Mander's maps (Matlab) graph the contribution of each pixel to the global coefficient:

$$MandersMap = \frac{(Im_{CFP} \times Im_{YFP}) \times 100}{M \times \sqrt{\sum (Im_{CFP})^2 \times \sum (Im_{YFP})^2}}. \quad (6)$$

Classification into high and low receptor expression levels

The classification into high and low expression levels was performed taking into account the mean of GFP signal (sum of GFP divided by cell size) of each cell. Cells with this value higher than 25 were considered to have high expression level, whereas cells with values lower than 20 were considered to have low expression level. In isoform discrimination of internalization, only the cells with a mean GFP signal <30 were considered in the quantification analysis in order to have an homogeneous cell sample for both isoforms.

Estimation of activation levels

We performed a similar analysis using Cy3 signal. After cell segmentation (membrane and interior) and mask generation, quantification of the Cy3 signal in the membrane of stimulated and non-stimulated cells was carried out. The ratio between this measurement and the membrane size (in pixels) was calculated for each cell. For evaluation of the expression level influence on receptor activation, a similar quantification was performed: the ratio between summed activation level (red) and summed expression level (green) signal in the membrane was calculated for each cell.

J.G. is a recipient of a CONICET fellowship and was awarded a short-term EMBO fellowship. This work was supported by the Max-Planck Society, University of Buenos Aires, CONICET (Argentina) and ANPCyT (Argentina). We thank Axel Ullrich for kindly providing plasmids pNTK2-hIR and pNTK2-IR/B, T. W. Gadella, Jr for pSCFP-3AC and pSYFP-2F vectors and Anabella Srebrow for the pCMV-AKT-HA vector. We thank Laboratorios BETA for providing rhIns. We thank Omar Coso for discussions about IR signaling and for providing the anti-ERK antibody and pCMV-β-Gal and AP-1-luc reporter plasmids and Patricia Cuasnicu for anti-PY20 antibody. We thank Wouter Caarls and Maria Julia Roberti for help and suggestions on Matlab use and figure preparation, respectively. We would like to thank Matías Blaustein for discussions about FRET experiments and Alejandro Colman Lerner for providing the anti-AKT antibody (Santa Cruz Biotechnology).

Supplementary material available online at
http://jcs.biologists.org/cgi/content/full/124/5/810/DC1

References

Andrews, N. L., Pfeiffer, J. R., Martinez, J. M., Haaland, D. M., Davis, R. W., Kawakami, T., Oliver, J. M., Wilson, B. S. and Lidke, D. S. (2009). Small, mobile Fc epsilon RI receptor aggregates are signaling competent. *Immunity* **31**, 469-479.

Backer, J. M., Kahn, C. R., Cahill, D. A., Ullrich, A. and White, M. F. (1990). Receptor-mediated internalization of insulin requires a 12-amino acid sequence in the juxtamembrane region of the insulin receptor β-subunit. *J. Biol. Chem.* **265**, 16450-16454.

Baily, C. E. M., Navé, B. T., Soos, M. A., Orr, S. R., Hayward, A. C. and Siddle, K. (1995). Insulin receptor/IGF-I receptor hybrids are widely distributed in mammalian tissues: quantification of individual receptor species by selective immunoprecipitation and immunoblotting. *Biochem. J.* **327**, 209-215.

Bhaskar, S., Surinya, K. H., Hadaschik, D. and Siddle, K. (2007). Characterization of insulin/IGF hybrid receptors: contributions of the insulin receptor L2 and Fn1 domains and the alternatively spliced exon 11 sequence to ligand binding and receptor activation. *Biochem. J.* **403**, 603-613.

Bergeron, J. J., Di Guglielmo, G. M., Baass, P. C., Authier, F. and Posner, B. I. (1995). Endosomes, receptor tyrosine kinase internalization and signal transduction. *Biosci. Rep.* **15**, 411-418.

Biener, Y., Feinstein, R., Mayak, M., Kaburagi, Y., Kadowaki, T. and Zick, Y. (1996). Annexin II is a novel player in insulin signal transduction. Possible association between annexin II phosphorylation and insulin receptor internalization. *J. Biol. Chem.* **271**, 29489-29496.

Blanquart, C., Achi, J. and Issad, T. (2008). Characterization of IRA/IRB hybrid insulin receptors using bioluminscence resonance energy transfer. *Biochem. Pharmacol.* **76**, 873-883.

Borisov, N., Aksamitiene, E., Kiyatkin, A., Legewie, S., Berkhout, J., Maiwald, T., Kaimachnikov, N. P., Timmer, J., Hoek, J. B. and Kholodenko, B. N. (2009). Systems-level interactions between insulin-EGF networks amplify mitogenic signaling. *Mol. Syst. Biol.* **5**, 256.

Cambi, A., Lidke, D. S., Arndt-Jovin, D. J., Figdor, C. G. and Jovin, T. M. (2007). Ligand-conjugated quantum dots monitor antigen uptake and processing by dendritic cells. *Nano Lett.* **7**, 970-977.

Ceresa, B. P., Kao, A. W., Santeler, S. R. and Pessin, J. E. (1998). Inhibition of clathrin mediated endocytosis selectively attenuates specific insulin receptor signal transduction pathways. *Mol. Cell. Biol.* **18**, 3862-3870.

Denley, A., Bonython, E. R., Booker, G. W., Cosgrove, L. J., Forbes, B. E., Ward, C. W. and Wallace, J. C. (2004). Structural determinants for high-affinity binding of insulin-like growth factor II to insulin receptor (IR)-A, the exon 11 minus isoform of the IR. *Mol. Endocrinol.* **18**, 2502-2512.

Di Guglielmo, G. M., Baass, P. C., Ou, W. J., Posner, B. I. and Bergeron, J. J. (1994). Compartmentalization of SHC, GRB2 and mSOS, and hyperphosphorylation of Raf-1 by EGF but not insulin in liver parenchyma. *EMBO J.* **13**, 4269-4277.

Ebina, Y., Ellis, L., Jarnagin, K., Edery, M., Graf, L., Clauser, E., Ou, J., Masiarz, F., Kan, Y. W., Goldfine, I. D. et al. (1985). The human insulin receptor cDNA: the structural basis for hormone-activated transmembrane signalling. *Cell* **40**, 747-758.

Echarte, M. M., Bruno, L., Arndt-Jovin, D. J., Jovin, T. M. and Pietrasanta, L. I. (2007). Quantitative single particle tracking of NGF-receptor complexes: transport is bidirectional but biased by longer retrograde run lengths. *FEBS Lett.* **581**, 2905-2913.

Frasca, F., Pandini, G., Scalia, P., Sciacca, L., Mineo, R., Costantino, A., Goldfine, I. D., Belfiore, A. and Vigneri, R. (1999). Insulin receptor isoform A, a newly recognized, high-affinity insulin-like growth factor II receptor in fetal and cancer cells. *Mol. Cell. Biol.* **19**, 3278-3288.

Goldstein, B. J. and Dudley, A. L. (1990). The rat insulin receptor: primary structure and conservation of tissue-specific alternative messenger RNA splicing. *Mol. Endocrinol.* **4**, 235-244.

Grimes, M. L., Zhou, J., Beattie, E. C., Yuen, E. C., Hall, D. E., Valletta, J. S., Topp, K. S., LaVail, J. H., Bunnett, N. W. and Mobley, W. C. (1996). Endocytosis of activated TrkA: Evidence that nerve growth factor induces formation of signaling endosomes. *J. Neurosci.* **16**, 7950-7964.

Haft, C. R., Sierra, M. L., Hamer, I., Carpentier, J. L. and Taylor, S. I. (1998). Analysis of the juxtamembrane dileucine motif in the insulin receptor. *Endocrinology.* **139**, 1618-1629.

Hagen, G. M., Caarls, W., Thomas, M., Hill, A., Lidke, K., Rieger, B., Fritsch, C., van Geest, B., Jovin, T. M. and Arndt-Jovin, D. J. (2007). Biological applications of an LCoS-based Programmable Array Microscope (PAM). *Proc. SPIE* **6441**, 64410S1-S12.

Hagen, G. M., Caarls, W., Lidke, K., de Vries, A. H. B., Fritsch, C., Barisas, B. G., Arndt-Jovin, D. J. and Jovin, T. M. (2009). Photoconversion and FRAP measurements in arbitrary regions of interest using a Programmable Array Microscope. *Microsc. Res. Tech.* **72**, 431-440.

Hamer, I., Foti, M., Emkey, R., Cordier-Bussat, M., Philippe, J., De Meyts, P., Maeder, C., Kahn, C. R. and Carpentier, J. L. (2002). An arginine to cysteine (252) mutation in insulin receptors from a patient with severe insulin resistance inhibits receptor internalization but preserves signalling events. *Diabetologia* **45**, 657-667.

Hari, J. and Roth, R. A. (1987). Defective internalization of insulin and its receptor in cells expressing mutated insulin receptors lacking kinase activity. *J. Biol. Chem.* **262**, 15341-15344.

Heintzmann, R., Hanley, Q. S., Arndt-Jovin, D. J. and Jovin, T. M. (2001). A dual path programmable array microscope (PAM): simultaneous acquisition of conjugate and non-conjugate images. *J. Microsc.* **204**, 119-135.

Jensen, M. and De Meyts, P. (2009). Molecular mechanisms of differential intracellular signaling from the insulin receptor. *Vitam. Horm.* **80**, 51-75.

Kellerer, M. G., Sesti, G., Seffer, E., Obermaier-Kusser, B., Pongratz, D. E., Mosthaf, L. and Häring, H. U. (1993). Altered pattern of insulin receptor isotypes in skeletal muscle membranes of type 2 (non-insulin-dependent) diabetic subjects. *Diabetologia.* **36**, 628-632.

Kremers, G. J., Goedhart, J., van Munster, E. R. and Gadella, W. J. (2006). Cyan and yellow super fluorescent proteins with improved brightness, protein folding, and FRET Förster Radius. *Biochemistry.* **45**, 6570-6580.

Lidke, D. S., Nagy, P., Heintzmann, R., Arndt-Jovin, D. J., Post, J., Grecco, H., Jares-Erijman, E. A. and Jovin, T. M. (2004). Quantum dot ligands reveal EGFR dynamics in living cells. *Nat. Biotechnol.* **22**, 198-203.

Lidke, D. S., Lidke, K., Rieger, B., Jovin, T. M. and Arndt-Jovin, D. J. (2005). Reaching out for signals: filopodia sense EGF and respond by directed retrograd transport of activated receptors. *J. Cell Biol.* **170**, 619-626.

Lidke, D. S., Nagy, P., Heintzmann, R., Jovin, T. M. and Arndt-Jovin, D. J. (2007). Biotin-ligand complexes with streptavidin quantum dots for in vivo cell labeling of membrane receptors. *Methods Mol. Biol.* **374**, 69-80.

McClain, D. A., Maegawa, H., Lee, J., Dull, T. J., Ullrich, A. and Ole[illegible]ky, J. M. (1987). A mutant insulin receptor with defective tyrosine kinase displays no biologi[illegible]ivity and does not undergo endocytosis. *J. Biol. Chem.* **262**, 14663-146[illegible].

McKeon, C., Moncada, V., Pham, T., Salvatore, P., K[illegible]owaki, T. Cecili, D. and Taylor, S. I. (1990). Structural and functional analysis of the insulin rec[illegible]or promoter. *Mol. Endocrinol.* **4**, 647-656.

Mosthaf, L., Grako, K., Dull, T. J., Coussens, L., Ullric[illegible]A. and McClain, D. A. (1990). Functionally distinct insulin recep[illegible]s generated by [illegible]ue-specific alternative splicing. *EMBO J.* **9**, 2409-2413.

Mosthaf, L., Vogt, B., Haring, H. [illegible]and Ullri[illegible]h, A. (1991). Altered expression of insulin receptor types A and B in the [illegible]eletal [illegible]uscle of non-insulin dependent diabetes mellitus patients. *Proc. Natl. Acad. Sci[illegible]* **88**, 4728-[illegible]730.

Pandini, G., Vigneri, R., C[illegible]o, A., F[illegible]ca, F., [illegible]olito, A., Fujita-Yamaguchi, Y., Siddle, K., Goldfine, I. D. an[illegible] Belfiore, [illegible]999). Insulin and insulin-like growth factor-I (IGF-I) re[illegible]or overev[illegible]ion in breast cancers leads to insulin/IGF-I hybrid receptor overexpress[illegible] ev[illegible]nce f[illegible]a second mechanism of IGF-I signaling. *Clin. Cancer Res.* **5**, 1935-19[illegible]

Pandini, G., Frasca, F., M[illegible]o, R., Sciacca, L., Vigneri, R. and Belfiore, A. (2002). Insulin/insulin-like growth factor I hybrid receptors have different biological characteristics depending on the insulin receptor isoform involved. *J. Biol. Chem.* **277**, 39684-39695.

Papa, V., Gliozzo, B., Clark, G. M., McGuire, W. L., Moore, D., Fujita-Yamaguchi, Y., Vigneri, R., Goldfine, I. D. and Pezzino, V. (1993). Insulin-like growth factor-I receptors are overexpressed and predict a low risk in human breast cancer. *Cancer Res.* **53**, 3736-3740.

Pastore, S., Mascia, F., Mariotti, F., Dattilo, C., Mariani, V. and Girolomoni, G. (2005). ERK1/2 regulates epidermal chemokine expression and skin inflammation. *J. Immunol.* **174**, 5047-5056.

Patti, M. E. and Kahn, C. R. (1998). The insulin receptor, a critical link in glucose homeostasis and insulin action. *J. Basic Clin. Physiol. Pharmacol.* **9**, 89-109.

Pol, A., Calvo, M. and Enrich, C. (1998). Isolated endosomes from quiescent rat liver contain the signal transduction machinery. Differential distribution of activated Raf-1 and Mek in the endocytic compartment. *FEBS Lett.* **441**, 34-38.

Reynet, C., Caron, M., Magre, J., Cherqui, G., Clauser, E., Picard, J. and Capeau, J. (1990). Mutation of tyrosine residues 1162 and 1163 of the insulin receptor affects hormone and receptor internalization. *Mol. Endocrinol.* **4**, 304-311.

Rizzo, M. A., Shome, K., Watkins, S. C. and Romero, G. (2000). The recruitment of Raf-1 to membranes is mediated by direct interaction with phosphatidic acid and is independent of association with Ras. *J. Biol. Chem.* **275**, 23911-23918.

Russell, D. S., Gherzi, R., Johnson, E. L., Chou, C. K. and Rosen, O. M. (1987). The protein-tyrosine kinase activity of the insulin receptor is necessary for insulin-mediated receptor down-regulation. *J. Biol. Chem.* **262**, 11833-11840.

Saltiel, A. R. and Kahn, R. (2001). Insulin signaling and the regulation of glucose and lipid metabolism. *Nature* **414**, 799-806.

Savkur, R. S., Philips, A. V. and Cooper, T. A. (2001). Aberrant regulation of insulin receptor alternative splicing is associated with ins[illegible]n resist[illegible]e in myotonic dystrophy. *Nat. Genet.* **29**, 40-47.

Sebastian, S., Settleman, J., Reshkin, S. J., Azz[illegible]i, A., Belliz[illegible]A. and Paradiso, A. (2006). The complexity of targeting E[illegible]FR signa[illegible]ing in canc[illegible]: from expression to turnover. *Biochem. Biophys. Acta* [illegible], 120-139.

Seino, S. and Bell, G. I. (1989). Al[illegible]native splicing of h[illegible] insulin receptor messenger RNA. *Biochem. Biophys. Res. C[illegible]mmun[illegible]*, 312-316.

Sen, S., Talukdar, I. and Webster[illegible]G. (2009). SRp20 and CUG-BP1 modulate insulin receptor exon [illegible] alternative [illegible]icing. *Mol. Cell. Biol.* **29**, 871-880.

Sorkin, A., Eriksso[illegible] Heldin, C. [illegible] Westermark, B. and Claesson-Welsh, L. (1993). Pool of ligand-bound platelet-derived growth factor beta-receptors remain activated and tyrosine phosphorylated after internalization. *J. Cell. Physiol.* **156**, 373-382.

Sorki[illegible]A., McClure, M., Huang, F. and Carter, R. (2000). Interaction of EGF receptor and grb2 in living cells visualized by fluorescence resonance energy transfer (FRET) microscopy. *Curr[illegible]iol.* **10**, 1395-1398.

Thies[illegible]S., Webste[illegible]N. J. and McClain, D. A. (1990). A domain of the insulin receptor required for endocytosis in rat fibroblasts. *J. Biol. Chem.* **265**, 10132-10137.

Uhles, S., [illegible], T., Leibiger, B., Berggren, P. O. and Leibiger, I. B. (2003). Isoform-specific insulin receptor signaling involves different plasma membrane domains. *J. Cell Bi[illegible]63*, 1327-1337.

Ullrich, A., Bell, J. R., Chen, E. Y., Herrera, R., Petruzelli, L. M., Dull, T. J., Gray, A., Coussens, L., Liao, Y., Tsubokawa, M. et al. (1985). Human insulin receptor and its relationship to the tyrosine kinase family of oncogenes. *Nature* **313**, 756-761.

Vogt, B., Carrascosa, J. M., Ermel, B., Ullrich, A. and Haring, H. U. (1991). The two isotypes of the human insulin receptor (HIR-A and HIR-B) follow different internalization kinetics. *Biochem. Biophys. Res. Commun.* **177**, 1013-1018.

Ward, C. W., Lawrencea, M. C., Streltsova, V. A., Adams, T. E. and McKern, N. M. (2007). The insulin and EGF receptor structures: new insights into ligand-induced receptor activation. *Trends Biochem. Sci.* **32**, 129-137.

White, M. F. (1998). The IRS-signalling system: a network of docking proteins that mediate insulin action. *Mol. Cell. Biochem.* **182**, 3-11.

Wilden, P. A., Backer, J. M., Kahn, C. R., Cahill, D. A., Schroeder, G. J. and White, M. F. (1990). The insulin receptor with phenylalanine replacing tyrosine-1146 provides evidence for separate signals regulating cellular metabolism and growth. *Proc. Natl. Acad. Sci. USA* **87**, 3358-3362.

Yamaguchi, Y., Flier, J. S., Yokota, A., Benecke, H., Backer, J. M. and Moller, D. E. (1991). Functional properties of two naturally occurring isoforms of the human insulin receptor in Chinese hamster ovary cells. *Endocrinology.* **129**, 2058-2066.

Yamaguchi, Y., Flier, J. S., Benecke, H., Ransil, B. J. and Moller, D. E. (1993). Ligand-binding properties of the two isoforms of the human insulin receptor. *Endocrinology.* **132**, 1132-1138.

Yamamoto-Honda, R., Koshio, O., Tobe, K., Shibasaki, Y., Momomura, K., Odawara, M., Kadowaki, T., Takaku, F., Akanuma, Y. and Kasuga, M. (1990). Phosphorylation state and biological function of a mutant human insulin receptor val996. *J. Biol. Chem.* **265**, 14777-14783.